NASA TECHNICAL NOTE

NASA TN D-6378

NASA TN D-6378

EXCITATION OF BOUNDARY-LAYER TURBULENCE THROUGH SPARK DISCHARGES

by Enrique J. Klein

Ames Research Center
Moffett Field, Calif. 94035

NATIONAL AERONAUTICS AND SPACE ADMINISTRATION • WASHINGTON, D. C. • MAY 1971

1. Report No.	2. Government Accession No.	3. Recipient's
NASA TN D-6378		

4. Title and Subtitle

EXCITATION OF BOUNDARY-LAYER TURBULENCE THROUGH SPARK DISCHARGES

5. Report Date: May 1971

6. Performing Organization Code:

7. Author(s)

Enrique J. Klein

8. Performing Organization Report No.: A-3673

9. Performing Organization Name and Address

NASA Ames Research Center
Moffett Field, Calif. 94035

10. Work Unit No.: 129-01-20-04-00-21

11. Contract or Grant No.:

12. Sponsoring Agency Name and Address

National Aeronautics and Space Administration
Washington, D. C. 20546

13. Type of Report and Period Covered: Technical Note

14. Sponsoring Agency Code:

15. Supplementary Notes

16. Abstract

An experimental investigation was made of the effect of spark discharges into a laminar boundary layer at supersonic free-stream Mach numbers. Flow visualization studies showed that a spark could generate a boundary-layer disturbance with a turbulent structure that grows as it is swept downstream. Local skin friction was measured by a floating element balance installed in a flat plate model downstream of a pair of electrodes embedded flush with the surface near the sharp leading edge. Tests were carried out in the Ames 1- by 3-Foot Supersonic Wind Tunnel at Mach numbers of 1.98, 2.56, 3.53 and 3.88, using spark discharge frequencies from 0 to 32,000 sparks per second. The local skin-friction coefficient c_f could be brought to a turbulent level in normally laminar and transitional boundary layer regions with the higher spark discharge frequencies. The resulting level of c_f was comparable to that obtained with spherical trips, or with normal turbulence, or from theory. The measured skin friction was found to be significantly affected by the spark discharge frequency, but little affected by changes in the energy per spark. The kinetic and thermal energy into the medium from a single spark was computed from experimental data by means of an available numerical solution. This energy was of the order of 1 percent of the electrical input to the spark.

17. Key Words (Suggested by Author(s))

Boundary layers
Boundary layer transition
Boundary layer trips
Spark discharges
Skin friction measurements

18. Distribution Statement

Unclassified – Unlimited

19. Security Classif. (of this report)	20. Security Classif. (of this page)	21. No. of Pages	22. Price*
Unclassified	Unclassified	17	$3.00

*For sale by the National Technical Information Service, Springfield, Virginia 22151

SYMBOLS

a	speed of sound, cm/s
C	capacitance, F
c_f	local skin-friction coefficient
$\bar{c}_f$	arithmetic mean of $c_{f_{max}}$ and $c_{f_{min}}$
E_{sp}	electrical energy into a single spark, J/spark
E_o	energy released by an explosion into a sphere, J
$E_\circ$	energy released by an explosion into a hemisphere, J
f	frequency of spark discharge, sparks/s
I_s	current at the power supply, A
k	skin-friction balance calibration constant, $(g/cm^2)/V$
l	dimensionless radius of a spherical shock wave (see eq. (8))
M_∞	free-stream Mach number
p_1	pressure ahead of a shock front, kg/cm^2
p_t	wind-tunnel total pressure, kg/cm^2
P_{sp}	electrical power into a train of sparks, W
q	wind-tunnel dynamic pressure, kg/cm^2
r_m	measured radius of a spherical shock wave, cm
Re_m	Reynolds number at the measuring station
Re_t	Reynolds number of transition
Re_x	Reynolds number referred to the distance from the virtual origin
Re_∞/cm	free-stream unit Reynolds number
$(Re_\infty/cm)_o$	unit Reynolds number for the origin of turbulence at the measuring station
t	dimensionless time for a spherical shock wave growth (see eq. (9))

t_m	measured time for growth of a spherical shock wave, μs
T_1	total temperature ahead of shock front, °K
V_s	power supply potential, V
V_{sp}	voltage across the capacitor, V
V_k	skin-friction balance output, V
V_o	skin-friction balance zero shift, V
x_m	distance from the leading edge to the measuring station, cm
η	efficiency of a single spark at static conditions
ρ_1	density ahead of a shock front, kg/cm^3
τ	local skin friction, g/cm^2

EXCITATION OF BOUNDARY-LAYER TURBULENCE THROUGH SPARK DISCHARGES*

Enrique J. Klein

Ames Research Center

SUMMARY

An experimental investigation was made of the effect of spark discharges into a laminar boundary layer at supersonic free-stream Mach numbers. Flow visualization studies showed that a spark could generate a boundary-layer disturbance with a turbulent structure that grows as it is swept downstream. Local skin friction was measured by a floating element balance installed in a flat plate model downstream of a pair of electrodes embedded flush with the surface near the sharp leading edge. Tests were carried out in the Ames 1- by 3-Foot Supersonic Wind Tunnel at Mach numbers of 1.98, 2.56, 3.53 and 3.88, using spark discharge frequencies from 0 to 32,000 sparks per second. The local skin-friction coefficient c_f could be brought to a turbulent level in normally laminar and transitional boundary layer regions with the higher spark discharge frequencies. The resulting level of c_f was comparable to that obtained with spherical trips, or with normal turbulence, or from theory. The measured skin friction was found to be significantly affected by the spark dishcarge frequency, but little affected by changes in the energy per spark. The kinetic and thermal energy into the medium from a single spark was computed from experimental data by means of an available numerical solution. This energy was of the order of 1 percent of the electrical input to the spark.

INTRODUCTION

In supersonic and hypersonic wind-tunnel experiments on aerodynamic models, Reynolds numbers are usually of about one order of magnitude less than occur at full scale, the implication being that the boundary layers on the wind-tunnel models will not necessarily correspond to those at full scale. Consequently, skin friction, heat transfer, flow separation, and the viscous interaction of the boundary layer with shock waves will generally not be representative of full-scale conditions. To compensate for this, attempts have been made for many years to promote boundary-layer transition, from laminar to turbulent, closer to the leading edge of a model than would occur spontaneously in a given facility at the test Reynolds number. Methods currently in use consist in attaching trips, usually grit, spheres, cylinders, or flat triangles, to the model surface close to the leading edge. Although the wave drag of conventional trips can apparently be accounted for (ref. 1), their capability to alter a laminar boundary layer so that it will correspond to a natural fully developed turbulent boundary layer has never been demonstrated. However, questions as to the validity of the use of trips have arisen from observations of: (a) the strong and persistent vortices in the boundary layer generated at the trips and made visible by the sublimation technique (ref. 2);

*This investigation was accomplished during the author's tenure of a National Research Council Postdoctoral Research Associateship supported by the National Aeronautics and Space Administration.

(b) the uneven temperature distribution in the cusped disturbance following a trip, as detected by the liquid crystal technique (ref. 3); and (c) the anomalies in the local skin friction downstream of grit of various sizes as measured with a skin-friction balance (ref. 4).

In most supersonic and hypersonic wind tunnels operating at their maximum Reynolds numbers, boundary-layer transition will occur several inches or even feet downstream of the leading edge of the model. Making a turbulent boundary layer start closely behind the leading edge of the model cannot be achieved by conventional trips. Trips act as continuous vortex generators, and while the presence of streamwise vorticity may be a sufficient condition for the generation of turbulence, the distance from the trip at which turbulence develops depends on the size of the trip, the flow Mach number, and the unit Reynolds number.

These considerations, plus the decrease in the effectiveness of trips as the Mach number is raised into the hypersonic range, prompted this investigation of a new and unconventional method for inducing turbulence in laminar boundary layers. To provide a basis for an experimental approach to this problem, it was necessary to look into the physical mechanism of boundary-layer transition.

The transition process has been studied in thick boundary layers at subsonic velocities (e.g., refs. 5 and 6), and its major phases are now well identified. It is assumed here that the same process occurs at supersonic and hypersonic velocities. Referring to the turbulent breakdown phase, the last phase of transition, the following important features have been recognized:

1. Boundary-layer turbulence is generated over a region of finite length.

2. The appearance of turbulent spots in the region mentioned in point 1 is an intermittent phenomenon.

3. Turbulent spots grow as they are carried downstream within the laminar boundary layer.

4. A turbulent boundary layer is formed when a sufficient number of turbulent spots coalesce.

Preliminary studies indicated that a concentrated and abrupt transition process could perhaps be achieved by the artificial excitation of turbulent spots near the leading edge of the model. This would mean starting the process in what corresponds to the last phase of normal transition. Such a method would require:

1. Generation of a discrete, localized pulse disturbance in the laminar boundary layer.

2. Periodic repetition of this pulse disturbance in the laminar boundary layer.

3. Spanwise distribution of the disturbance sources.

The only known method for artificially generating turbulent spots in laminar boundary layers, although in subsonic flow only, was reported by M. Mitchner (ref. 7), G.B. Schubauer and P.S. Klebanoff (ref. 8), and J.W. Elder (ref. 9). It consists in discharging electrical sparks across the boundary layer from an electrode to the model surface. The use of a system of high-frequency spark discharges appeared to offer the most promising solution.

In this investigation, pulse disturbances were introduced into the boundary layer by sparks discharged across a pair of electrodes embedded flush with the model surface. The electric arc between the electrodes occurs for about 0.1 microsecond. During this time the high vacuum in the arc plasma causes the plasma to act as a temporary solid obstruction to the flow, thus introducing a pulse disturbance into the boundary layer. The purpose of this method should not be confused with that of studying the complete transition process by generating or enhancing small perturbations in the laminar boundary layer flow by means of a vibrating ribbon (ref. 10), an intermittent air jet from the surface (ref. 11), or an electrical glow discharge at high frequency (ref. 12).

The above proposed method is an attempt to artificially induce early boundary-layer turbulence which will correspond to normal boundary-layer turbulence. It is recognized, however, that the method introduces uniformly intermittent disturbances which may behave differently from the more random turbulent spots which appear in the last phase of normal transition. The findings of this report are exploratory and are meant to provide a basis for more detailed investigations into the physical phenomena involved and into the possible usefulness of the method in wind-tunnel modelling.

DISTURBANCE VISUALIZATION

Tests were made in the 1- by 3-foot supersonic wind tunnel to observe the boundary-layer disturbance caused by single spark discharges.

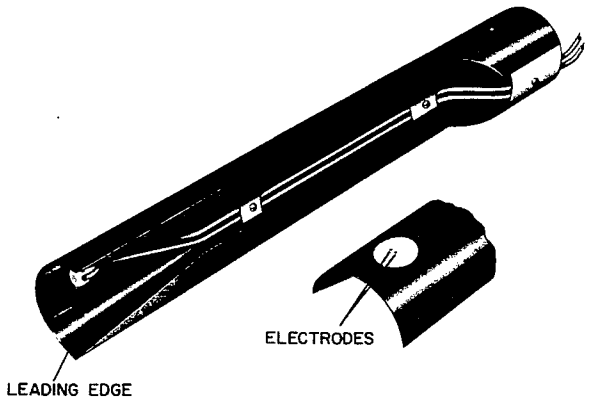

Figure 1.- Half-cylinder model, 5.08 cm in diameter, with a pair of tungsten electrodes flush with the surface and 2.22 cm from the leading edge.

A flat plate model with a sharp leading edge was used in the initial tests. This model proved inadequate since the boundary-layer disturbance from the spark discharge of a single pair of electrodes on its centerline was masked by the boundary layer on the entire width of the model. Good results were obtained with the half-cylinder model shown in figure 1. The model was 34.3 cm long and its half-cylindrical section had a 2.54 cm radius. A sharp leading edge of 0.0127 cm thickness was obtained by machining a cone out of the front end of the model. The two electrodes were alined normal to the direction of flow and were located 2.22 cm behind the leading edge. The electrodes were 0.076 cm diameter tungsten rods, spaced 0.19 cm at the surface. They were embedded in a boron nitride holder, and the entire assembly was flush with the model surface. The electrode supports were arranged so that the electrodes could be pushed out as they wore down.

Two optical systems were used in these tests: a simple shadowgraph and a focused shadowgraph. While the first system provided sharp images on 50.8×50.8 cm sheet film, the focused shadowgraph had the advantage of providing parallel light across the test section, thus reducing the distortion of the image. In the second system, an aperture at the focal point of the second mirror

minimized fogging of the film due to radiation from the sparks since the light emitted in the test section is grossly out of focus in that plane. Reducing the amount of extraneous light becomes important when tests are made at high frequency spark discharges or with a continuous arc discharge. Further, with this system, the entire flow field was imaged on a 10.2X12.7 cm screen that permitted the use of Polaroid film.

For single spark tests, the spark discharge circuit consisted of an R-C circuit controlled by a thyratron tube. Synchronization was arranged so that opening the shutter (in the focused shadowgraph system) would sequentially trigger the model spark and the shadowgraph spark gap. The delay between the model spark and the shadowgraph spark gap could be adjusted from 0 to 500 μs.

Figure 2 shows shadowgraphs of the half-cylinder model with the disturbance excited by a spark, photographed at 67 and 160 μs delays between the model spark discharge and the shadowgraph spark gap flash, respectively. The total energy stored to produce the spark was 0.32 joule; the test was carried out at $M_\infty = 3.53$. and $Re_\infty/cm = 1.63X10^6$. The model was set at zero angle of attack and the flow was from left to right. The boundary-layer disturbance originated by the model spark is clearly visible. It is thicker than the surrounding boundary layer, grows as it is carried downstream, and has a turbulent texture. The growth of the disturbance occurs mostly in the upstream direction. The downstream end of the disturbance generally lags behind the center of the hemispherical shock wave generated by the spark discharge as would be expected, since the disturbance moves in the slower boundary layer. The disturbance resembles the turbulent spots observed on models tested in a ballistic range (ref. 13). It should be noted that the boundary-layer turbulence at the extreme right of the shadowgraphs corresponds to the coalescence of turbulence generated at the two corners of the model's leading edge which curl around the model surface. This phenomenon was verified by the sublimation flow visualization technique.

A series of tests with this arrangement, and the spark circuit energy set variously at 2.65, 1.45, 0.32, and 0.12 joules, showed that at each setting, the spark was strong enough to excite a growing boundary-layer disturbance. As the energy input increased, the outer edge of the boundary-layer disturbance became more sharply delineated, and at 2.65 joules, what appeared to be a turbulent nucleus protruded above the normally flat edge of the disturbance at its downstream end. No noticeable difference in the thickness of the disturbance at each station could be detected when the spark energy input changed.

To study the formation and growth of these boundary-layer disturbances viewed against the surface of the model (not across its edge), a planview shadowgraph arrangement was devised. It consisted of a focused shadowgraph incorporating a plane mirror which served simultaneously as a flat plate model. This arrangement, although in itself successful, proved inadequate for observing any but the strongest disturbances because of the masking effect of the boundary layer on the wind-tunnel window (ref. 14).

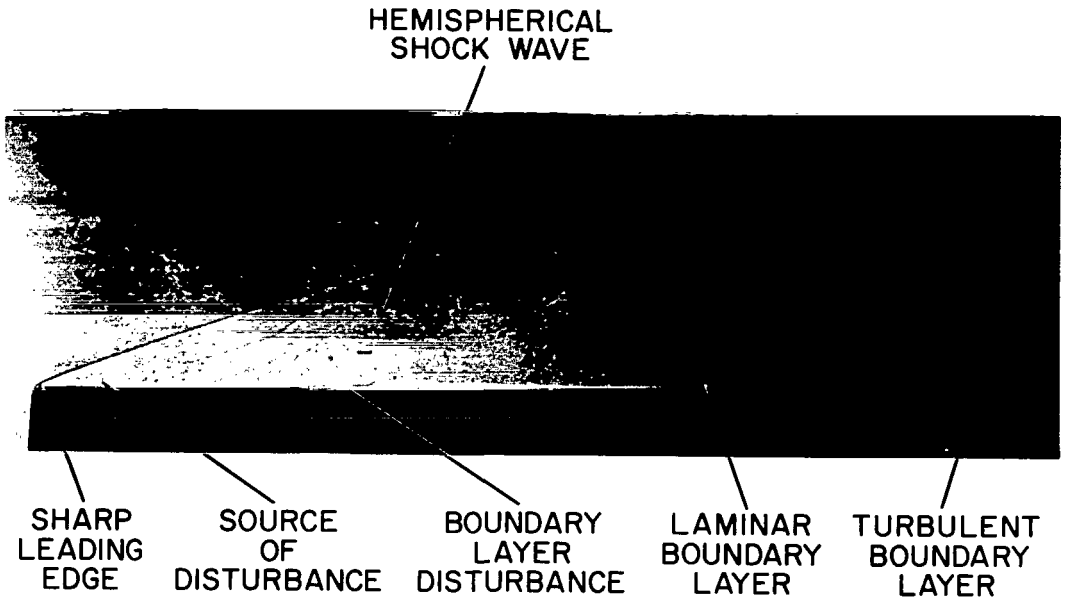

(a) 67 μs after spark discharge.

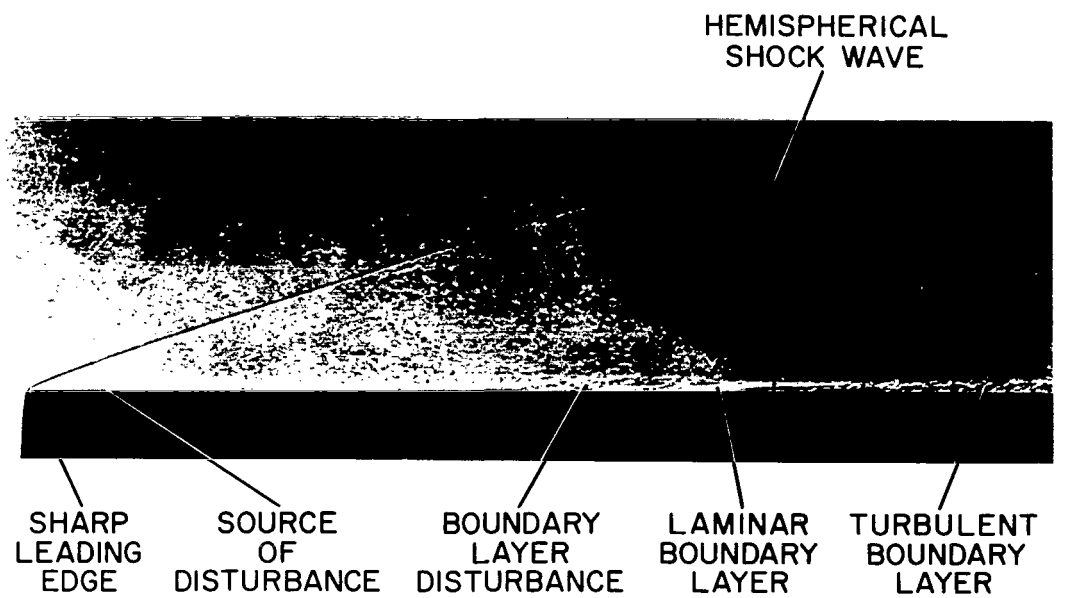

(b) 160 μs after the spark discharge.

Figure 2.- Shadowgraphs of the growth of the disturbance generated by a spark of 0.32 J in the boundary layer of a half-cylinder model at $M_\infty = 3.53$ and $Re_\infty/cm = 1.36 \times 10^5$.

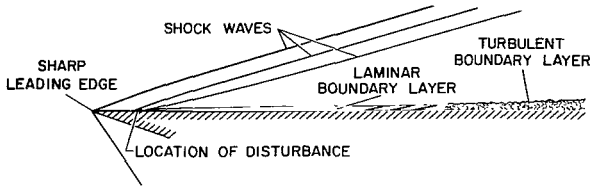

Figure 3.- Diagram of the boundary layer following a continuous disturbance source such as a roughness particle or a DC arc.

Additional tests were made, first with a 0.079 cm diameter sphere attached to the surface of the half-cylinder model and then with a continuous arc across the electrodes at a power of 250 and 188 W, to determine the effects of other disturbance mechanisms on the excitation of turbulence in boundary layers. Figure 3 shows features common to both the sphere and the continuous arc disturbances. Two weak shock waves are shown originating at the location of the disturbance. As in the case of the sphere, the boundary layer following the continuous arc is thicker than the undisturbed boundary layer. Increasing the power of the arc increases the thickness of the disturbed boundary layer, as when the sphere size is increased. This comparison suggests that the disturbance mechanism of a continuous arc may be similar to that of a solid particle. The dissimilarity between the effect of solid particles and sparks discharged at a high repetition rate into a boundary layer will be discussed in a later section.

EXPERIMENTAL ARRANGEMENTS

An experiment was designed to measure skin friction on a flat plate, downstream of a spark discharged at a high repetition rate into the boundary layer. Such measurements could then be compared with similar measurements made downstream of a row of conventional spherical trips, as well as with accepted semiempirical theories for turbulent skin friction on a flat plate.

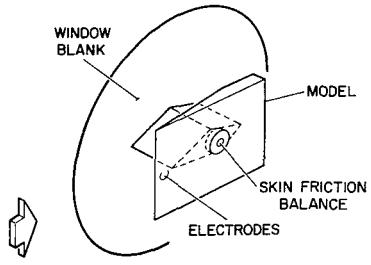

Figure 4.- Side-wall mounting of an instrumented flat plate model in the test section of the Ames 1- by 3-Foot Supersonic Wind Tunnel.

Because of the height of the available skin-friction balances (5.71 cm), a side-wall mounted arrangement was chosen which allowed the entire body of the balance to be enclosed inside a diamond-shaped supporting strut (see fig. 4). The model was 20.3 cm wide and 25.4 cm long, and was mounted with its flat surface at the center of the tunnel, at zero angle of attack, with its leading edge normal to the direction of flow. The leading edge was 0.0127 cm thick. The electrodes were alined normal to the direction of flow and were located 2.22 cm behind the leading edge. Their dimensions were the same as those in the half-cylinder model. The skin-friction balance was mounted flush with the model surface, 12.7 cm downstream of the electrodes. These dimensions insured that at the lowest Mach number tested (M_∞ = 1.98), the disturbance from the corners of the model would not reach the measuring element of the balance, while the entire element would be covered by the boundary-layer disturbance from the train of sparks (assuming a spreading angle of 11°).

The skin-friction balances[1] used in these experiments had a nominal range of 0 to 1.0 g/cm^2 for a full scale output of 5 V. These balances have a floating element flush with the surface,

[1] Kistler Instrument Corp. Model 322M102.

mounted on a beam suspended by flexural pivots. When an external force is applied to the floating element parallel to its surface and coincident with its direction of operation, a nulling servo-system keeps the element centered. The current required to produce the correcting force passes through an external load resistor, and the voltage across this resistor represents the output of the instrument. The calibration of these balances consisted in hanging different weights from the floating element and recording the voltage output indicated by a digital voltmeter. The linear calibration constants for the two balances used were 0.1946 and 0.1937 $(g/cm^2)/V$. Linearity deviation was within 1.6% at three times full scale (permissible with these balances). Calibration repeatability was 0.1% or better at nominal full scale. Zero shift was typically -0.004 g/cm^2 for one balance and half that value for the other.

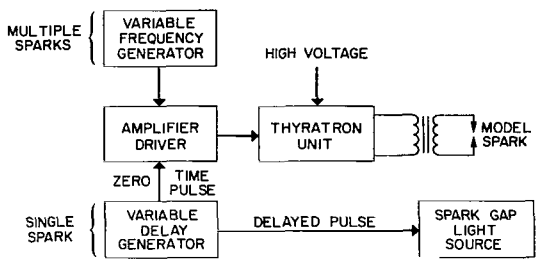

Figure 5.- Arrangement of the electronic equipment used to produce sparks.

Figure 5 is a block diagram of the electronic components for producing both single sparks and sparks at a high repetition rate. Multiple sparks are produced by a variable frequency generator capable of giving signals from 1 to 40 kHz. These signals are amplified and fed to the driver stage of the thyratron tube. The driver stage further amplifies them to 600 V pulses which then trigger the thyratron output. The thyratron unit includes a 1500 pF capacitor, which stores energy and discharges each time the thyratron tube is triggered. The voltage on the capacitor could be varied from about 3,000 to 10,000 V to change the energy input into the sparks. The isolation transformer following the thyratron unit was used to float the model electrically and prevent spark discharges from the electrodes to the model across the insulating boron nitride electrode holder. At tunnel static pressures of 0.0345 kg/cm^2 and below, some glow discharge was observed together with the spark discharge. As the pressure was decreased further, steady spark discharges could no longer be maintained. Sometimes at these low pressures, secondary sparks were also observed jumping sporadically from the electrodes to the rim of the electrode holder. The polarity of the connection to the electrodes is unimportant except that the erosion will take place preferentially on one of the electrodes. Electrode erosion was found to be minimal.

SKIN-FRICTION MEASUREMENTS

Preliminary tests were made at $M_\infty = 2.56$ and $Re_\infty/cm = 5.5 \times 10^4$ to determine the influence of the energy per spark on the skin-friction coefficient. Skin-friction measurements were made at spark discharge frequencies of 1,000, 2,000, 4,000, 8,000, 16,000, and 32,000 sparks/s. Three energy levels were tested. The energy per spark was computed from

$$E_{sp} = \frac{CV_{sp}^2}{2} \tag{1}$$

where C is the capacitance in farads, V_{sp} is the voltage measured across the capacitor, and E_{sp} results in joules per spark. The power input into the train of sparks was calculated from

$$P_{sp} = E_{sp}f \tag{2}$$

where f is the frequency of discharge in sparks per second, E_{sp} is given in joules per spark, and P_{sp} results in watts. The energy and power levels for a frequency of 32,000 sparks per second are listed in table 1.

TABLE 1.- ENERGY LEVELS AT 32,000 SPARKS PER SECOND

V_s, V	I_s, A	V_{sp}, V	E_{sp}, J/spark	P_{sp}, W	E_{sp}/E_{max} (approx.)
3,200	0.416	5,000	0.0188	600	1.0
2,200	.294	3,600	.0097	310	.5
1,550	.199	2,500	.0047	150	.25

Results showed that decreasing the energy level from 0.0188 to 0.0047 J/spark (a factor of 4) reduced the skin-friction coefficient only 2 percent. The maximum reduction of 8.7 percent occurred at 8000 sparks/s. (Increasing the energy above 0.0188 J/spark appeared to have a small effect on the skin-friction coefficient; decreasing the energy below 0.0047 J/spark was not practical since spark discharges were not stable below 1550 V.) Following this experiment, spark discharge tests were carried out at an energy level setting of 0.0047 J/spark.

Skin friction was measured at Mach numbers 1.98, 2.56, 3.53, and 3.88 over the available range of free-stream unit Reynolds numbers in the 1- by 3-foot supersonic wind tunnel. The following conditions were covered:

1. No boundary-layer disturbance,

2. Multiple spark discharges at 1,000, 2,000, 4,000, 6,000, 8,000, 16,000 and 32,000 sparks/s, and

3. A row of 0.079 cm diameter spheres attached to the model surface 2.22 cm downstream of the leading edge (like the electrodes), spaced at three diameters between centers.

The results are given in the logarithmic plots of skin-friction coefficient versus free-stream unit Reynolds number of figure 6. (Curves for some spark discharge frequencies have been omitted for greater clarity.) Also included in the graphs are the theoretical curves for a fully turbulent boundary layer computed according to the Van Driest II method (ref. 15) for adiabatic conditions, turbulent flow starting at the leading edge, and a length of turbulent flow of 14.91 cm (the distance from the leading edge to the centerline of the skin-friction balance).

The skin-friction coefficients were calculated from the experimental data using the equation

$$c_f = 0.001(\tau/q) \tag{3}$$

The dynamic pressure q was calculated from M_∞ and p_t, and the local shear from

$$\tau = k(V_k - V_o) \tag{4}$$

A sampling technique was used in recording the skin-friction balance output V_k, and an average from seven values was calculated. The amplifier had a low-pass filter with a 25 Hz cutoff and readings were delayed by 0.5 second.

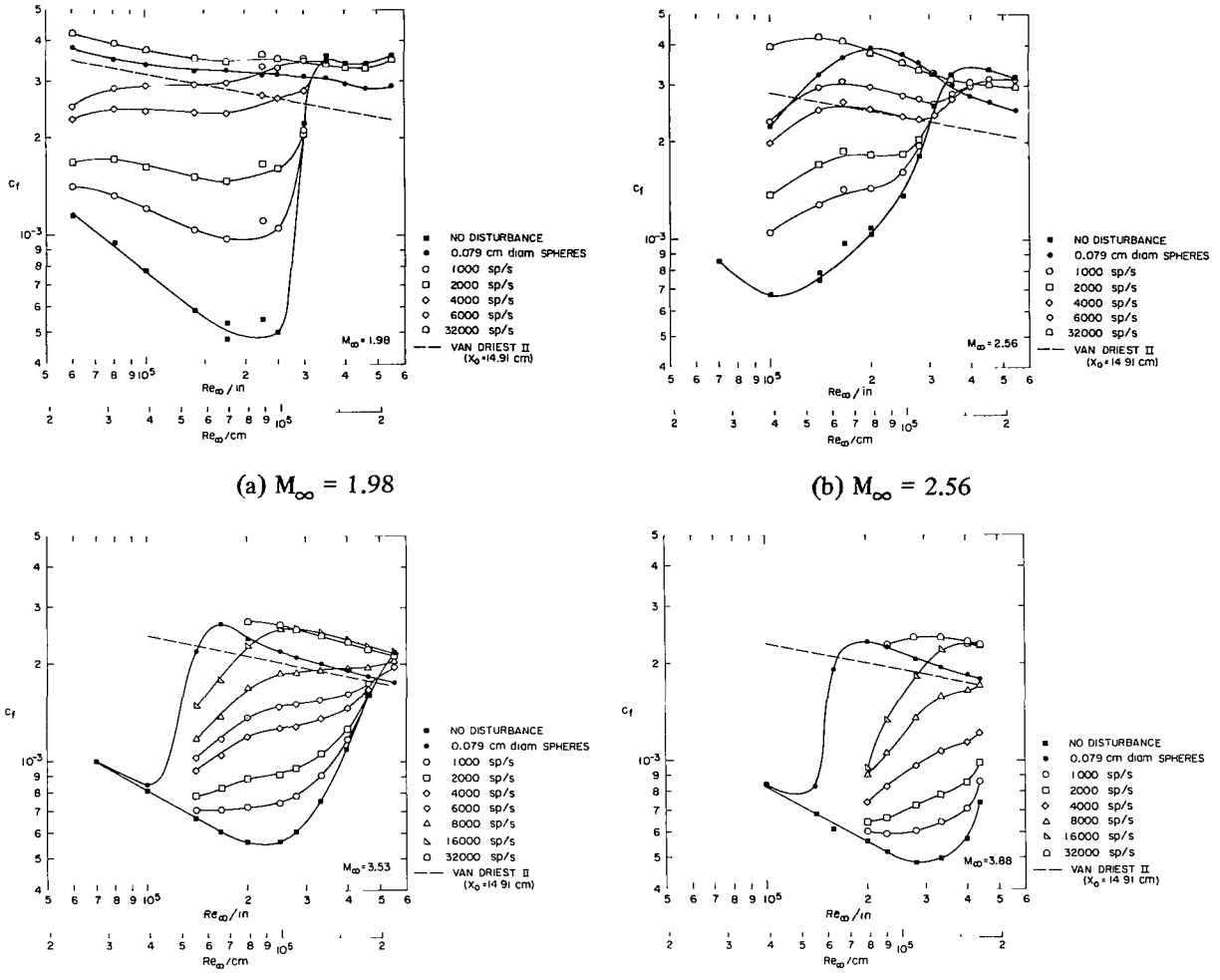

(a) $M_\infty = 1.98$

(b) $M_\infty = 2.56$

(c) $M_\infty = 3.53$

(d) $M_\infty = 3.88$

Figure 6.- Skin-friction coefficients versus wind tunnel unit Reynolds number for an instrumented flat plate model at zero angle of attack with a 0.0127 cm thick leading edge at zero sweep.

All measurements of local skin friction were made at one station only, 14.91 cm downstream of the leading edge, while the variation of the unit Reynolds number was obtained mainly by altering the total pressure of the wind-tunnel air. This implies that the graphs of figure 6 are not equivalent to a conventional plot of c_f versus Re_x, where Re_x is the Reynolds number referred to the distance from the leading edge. A tranformation to make possible a more direct comparison of these data with theoretical curves of c_f versus Re_x will be discussed later.

In the graphs of figure 6, the c_f curves for the 0.079 cm diameter spheres (filled circles) show that these trips lower the unit Reynolds number at which transition takes place. The highest frequency of spark discharges appears to cause a similar lowering of the unit Reynolds number at which transition takes place. As the frequency of discharge is increased, a point is reached where further increases in frequency will have no significant effect on c_f, probably because of the coalescence of turbulent spots. This saturation was observed over a range of unit Reynolds numbers

for 8,000, 16,000, and 32,000 sparks/s at $M_\infty = 1.98$ and 2.56 (these plots do not present the 8,000 and 16,000 sparks/s data for the sake of clarity), and for 16,000 and 32,000 sparks/s at $M_\infty = 3.53$. Nevertheless, the level of c_f was not coincident over the entire range of unit Reynolds numbers for the frequencies that produced saturation. For the highest spark discharge frequencies, the c_f level was higher than for the spheres and theory.

No clear law for the increase in skin-friction coefficient with frequency could be inferred from the available data. This is partly due to the nonlinear addition of the partial turbulence in the transitional boundary layer and the spark induced disturbances, to spark instability and glow discharge at the lower unit Reynolds numbers, and to the use of a balance designed for steady-state measurements. The inability to maintain a steady spark discharge at the lowest wind-tunnel static pressures is responsible for the data cutoff at low unit Reynolds numbers. The advent of instability depends on the free-stream Mach number, tunnel static pressure, and spark discharge frequency.

In figure 6(b) it was observed that high frequency spark discharges were able to reduce skin-friction coefficients somewhat at unit Reynolds numbers at which normally turbulent boundary layers resulted at the measuring station.

To permit a valid comparison of the experimental data with theoretical curves for a fully turbulent boundary layer, the data measured at one station may be transformed into a plot of c_f versus Re_x, the Reynolds number referred to the distance from the virtual origin. Then Re_x is defined as

$$Re_x = Re_m - Re_t \tag{5}$$

where Re_m is the Reynolds number at the measuring station given by

$$Re_m = (Re_\infty/cm)x_m \tag{6}$$

where x_m is the distance from the measuring station to the leading edge in cm; and

$$Re_t = (Re_\infty/cm)_o x_m \tag{7}$$

where $(Re_\infty/cm)_o$ is the unit Reynolds number at which the origin of turbulence coincides with the location of the measuring station. Substituting equations (6) and (7) into equation (5) results in

$$Re_x = x_m[(Re_\infty/cm) - (Re_\infty/cm)_o] \tag{8}$$

The unit Reynolds number effect was not considered in this transformation because it is not known how it would affect artificial transition processes as occur with spherical trips and sparks. Furthermore, its effect on the correlation is bound to be small because of the flat slope of the theoretical expression for c_f versus Re_x in the turbulent boundary-layer regime. This effect can be substantiated by data on the effect of unit Reynolds number on the Reynolds number of transition as measured in the same wind tunnel (ref. 16).

The value of $(Re_\infty/cm)_o$ for each experimental condition (i.e., no boundary-layer disturbance; spark discharges; and spheres) was taken at the arithmetic mean of c_f for the minimum and the peak of transition. These values were obtained, partly by extrapolation, from the data in figure 6

for $M_\infty = 2.56$ and 3.53. No transition peaks were visible for sparks and spheres at $M_\infty = 1.98$, and data were insufficient at $M_\infty = 3.88$ for sparks and for regular transition at the higher unit Reynolds numbers. Data used in determining $(Re_\infty/cm)_o$ are given in table 2 below:

TABLE 2.- $(Re_\infty/cm)_o$ FOR THE ORIGIN OF TURBULENCE

For $M_\infty = 2.56$	$c_{f_{min}}$	$c_{f_{max}}$	$\overline{c_f}$	$(Re_\infty/cm)_o$
No disturbance	0.00067	0.00346	0.00206	1.14×10^5
Spheres, 0.079 cm diam	.0011*	.00392	.00251	4.3×10^4
Sparks at 32,000 sparks/s	.0014*	.00425	.00282	2.8×10^4
For $M_\infty = 3.53$				
No disturbance	.00055	———	———	———
Spheres, 0.079 cm diam.	.00085	.00268	.00176	5.1×10^4
Sparks at 32,000 sparks/s	.00125*	.00274	.00199	4.9×10^4

*Extrapolated value

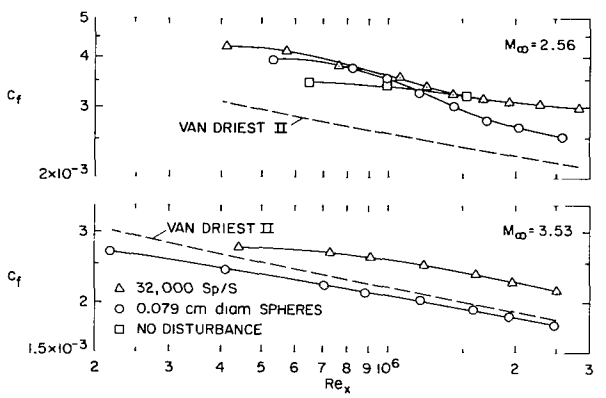

Figure 7.- Skin-friction coefficients versus the Reynolds number referred to the distance from the leading edge on a flat plate.

Figure 7 shows plots of c_f versus Re_x for the transformed experimental data and the theoretical curve for a fully developed boundary layer at adiabatic conditions following the Van Driest II method at $M_\infty = 2.56$ and 3.53. Only data at unit Reynolds numbers greater than that for each transition peak were used. The three points of regular transition near the peak at $M_\infty = 2.56$ (the only data available) are included for additional reference. Note that the curves for spheres always remain below the spark discharge curves. This may be explained by any of the following possibilities:

1. Providing the origin of turbulence is considered to be at the same location for both sparks and spheres, sparks would appear to increase the momentum thickness less than the spheres, thus introducing a smaller disturbance into the boundary layer.

2. Assuming that the boundary layers following the sparks and the spheres are both fully turbulent, the effective length of turbulent flow is shorter for the sparks than for the spheres.

3. While skin friction was measured behind a row of spheres, the corresponding measurement with sparks was made behind only one pair of electrodes allowing for lateral gradients in the momentum distribution.

CONCLUDING REMARKS

Measurements of mean local skin friction on a flat plate downstream of a spark discharge location showed a large dependence on the frequency of discharge. A saturation limit of skin friction was found to take place at frequencies above a minimum determined mainly by the Mach number. The skin-friction coefficients obtained with spark generated disturbances at high repetition rates in normally laminar and transitional regions, were comparable in order of magnitude to those obtained with spherical trips and to theoretically determined values.

The energy used for each spark discharge had a very small effect on the resulting skin-friction coefficients. The efficiency of the spark discharge, in terms of the kinetic and thermal energy into the flow referred to the electrical energy input to the spark, was very small and somewhat dependent on the tunnel static pressure.

The results of this exploratory investigation have provided some insight into the behavior of such artificially disturbed boundary layers. However, a number of aspects of this experimental method require further research, particularly those dealing with the physical differences between laminar and transitional boundary layers disturbed by this method, and normally turbulent boundary layers.

Ames Research Center
National Aeronautics and Space Administration
Moffett Field, Calif., 94035, Jan. 13, 1971

APPENDIX

ENERGY BALANCE

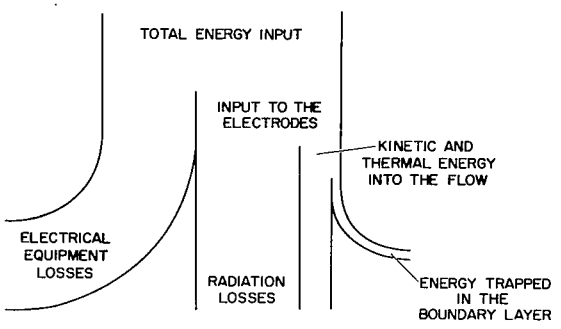

Figure 8.- Schematic diagram of the energy distribution of a spark discharge into the boundary layer of a wind tunnel model.

The energy distribution in a spark discharge system is shown in the diagram of figure 8. The input to the electrodes is divided into radiation losses and the kinetic and thermal energy added to the flow, a portion of which is assumed to become trapped in the boundary layer contributing to its turbulent growth.

In practice, it was not possible to determine all energy fractions. The total energy input into a single spark was determined from equation (1) using the capacitance and the voltage measured at the capacitor. The total kinetic and thermal energy into a quiescent medium from a single spark was obtained by applying a numerical solution (ref. 17), to the data of radius versus time of growth of the hemispherical shock wave generated by a spark discharge at the model. Direct measurements of current and voltage at the electrodes were not carried out because of the difficulties encountered with electrical noise and the inductance of the power carrying leads. The radiation energy emitted by the spark, which can represent a large proportion of the total energy, is extremely difficult to measure because of the strong absorption of the light of shorter wavelengths in the surrounding air. A method was also tried, by which the kinetic and thermal energy of a single spark discharge into the medium would be computed by means of Sedov's solution (ref. 17), both for static and running conditions, using the same total energy per spark and tunnel static pressure. The energy difference between the two cases would then have corresponded to the energy trapped in the boundary layer. Results were inconclusive because measurements obtained with the wind tunnel in operation did not agree with Sedov's numerical solution. The discrepancies could be attributed to factors such as the inaccuracy of the shock radii measurements due to the angularity of flow, and inaccuracy in the static temperature determination from the free-stream Mach number and the total temperature due to nonisentropic flow.

The focused shadowgraph arrangement was used in conjunction with the single spark discharge system (fig. 5) to determine the growth of the hemispherical shock wave generated by the spark. With the model installed in the wind-tunnel test section, the entire tunnel sealed and evacuated, single sparks were discharged and shadowgraphs were taken at preset time delays following the spark. The radii of the hemispherical shock waves visible in the 10.2X12.7 cm negatives were later measured with a digital optical comparator with a 0.0025 cm resolution. The initial measurements were made using the half-cylinder model of figure 1. However, since the lowest pressure attainable in the Ames 1- by 3-Foot Wind Tunnel under static conditions (around 0.10 kg/cm^2) is higher than the static pressures that occur when the tunnel is running, an additional sealed chamber, which

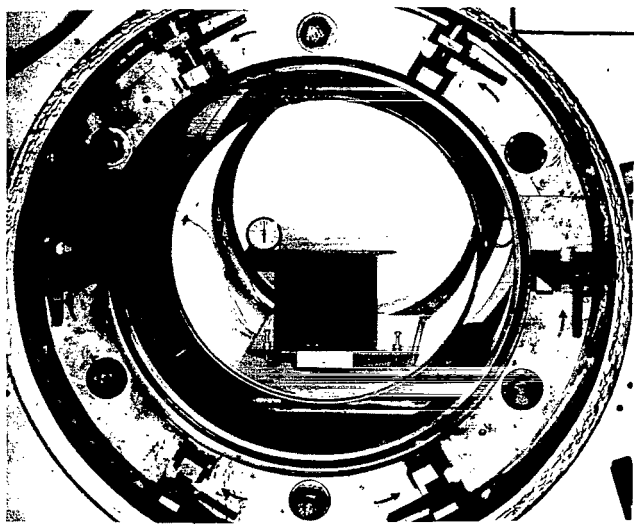

Figure 9.- Flat plate model inside a cylindrical chamber sealed into the test section of the Ames 1-by 3-Foot Supersonic Wind Tunnel, shown with the window removed. Configuration used for static testing.

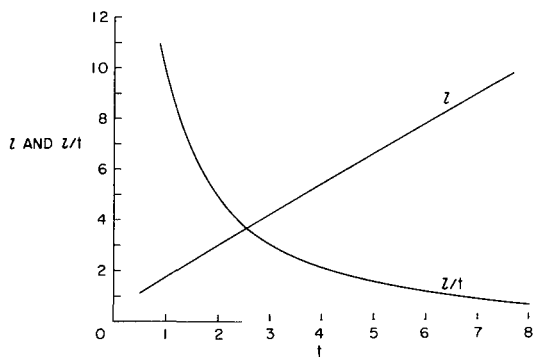

Figure 10.- Numerical solution for the growth with time of a spherical shock wave generated by a point explosion, taking counterpressure into consideration.

could be independently evacuated, was installed around the model in the test section. Figure 9 shows the arrangement in the tunnel test section with the north window removed. It consists of a 50.8 cm diameter steel tube sealed by "O" rings against the test section windows, a flat plate instrumented model mounted on a base with a three point support for levelling purposes, and a bimetallic thermometer for measuring the air temperature. The limitations of this technique were the loss in shock wave definition on the negative when the energy per spark was reduced and the pressure in the test chamber was decreased. The definition also suffered in shadowgraphs taken at the larger time delays since the energy input occurs only during the spark discharge, so that the shock wave weakens as it grows.

Sedov's numerical solution is for a point explosion in a perfect gas of constant initial density and pressure, larger than zero. The solution is given in terms of l, the dimensionless radius of the growing spherical shock wave. Figure 10 is a plot of l versus t and l/t versus t. The expressions for l and t are

$$l = \frac{r_m}{(E_o/p_1)^{1/3}} \tag{A1}$$

$$t = \frac{t_m}{E_o^{1/3} \rho_1^{1/2} p_1^{-5/6}} \tag{A2}$$

and the dimensionless ratio of l/t is obtained as

$$\frac{l}{t} = \frac{r_m}{t_m}\left(\frac{\rho_1}{p_1}\right)^{1/2} = \frac{r_m}{t_m}\,\frac{[\gamma]^{1/2}}{a} \tag{A3}$$

where a is the speed of sound; then

$$\frac{l}{t} = 590\left(\frac{r_m}{t_m}\right)\frac{1}{\sqrt{T_1}} \tag{A4}$$

using 1.4 for the ratio of specific heats for air.

The kinetic and thermal energy released by the spark discharge into a space bound by a plane and half of a spherical shock wave can be obtained as one half of E_o. From equation (A1)

$$E_\alpha = \frac{1}{2}E_o = \frac{1}{2}\,p_1\left(\frac{r_m}{l}\right)^3 \tag{A5}$$

or

$$E_{\Delta} = 0.0491\ p_1 \left(\frac{r_m}{l}\right)^3 \tag{A6}$$

using the units given in "Symbols." An equivalent result can be obtained by solving for E_0 in equation (A2).

To verify the correspondence of Sedov's solution with the experimental results obtained under static conditions, a single data point of r_m and t_m was chosen as a reference point, and Sedov's solution was used to reconstruct the entire experimental curve. The agreement between the rest of the data points and the reconstructed experimental curves was excellent.

The procedure for the computation of E_{Δ} consisted in:

1. Plotting r_m versus t_m and fairing a curve through the data points.

2. Choosing one point on the curve, preferably in the linear portion at the larger values of t_m.

3. Calculating l/t from equation (A4) and determining l and t from the graph of figure 10.

4. Computing E_{Δ} from equation (A6).

Computations of E_{Δ} were made for several values of the electrical energy input into a single spark E_{sp}. Results, including the efficiency of the spark under static conditions, are given in table 3.

TABLE 3.- SPARK EFFICIENCY – STATIC CONDITIONS

p_1, kg/cm^2	T_1, °K	C, pF	V_{sp}, V	E_{sp}, J	E_{Δ}, J	η, percent
0.157	293.1	35,800	9,000	1.450	0.00689	0.5
.157	293.1	8,000	9,000	.320	.00282	.9
.099	291.8	1,500	3,500	.0092	.00035	3.8
.048	292.1	1,500	3,500	.0092	.00017	1.8

In table 3, E_{sp} is calculated from equation (1), and the efficiency is defined as

$$\eta = \frac{E_{\Delta}}{E_{sp}} 100 \tag{A7}$$

For a typical experiment in which

$$C = 1{,}500 \text{ pF}$$

$$V_s = 1{,}550 \text{ V}$$

$$f = 32{,}000 \text{ sparks/s}$$

the current at the power supply and the voltage across the capacitor were

$$I_S = 0.234 \text{ A}$$

$$V_{sp} = 2{,}400 \text{ V}$$

As these values are practically independent of the Mach number and unit Reynolds number, taking as an example a test at $M_\infty = 2.56$ and $Re_\infty/cm = 1.57 \times 10^5$ in which $p_1 = 0.096$ kg/cm^2 the power levels can be computed as follows: The total power input to the equipment is given by $V_S I_S$, resulting in 363 W. The power into the train of sparks is given by equation (2) resulting in 138 W. Now, assuming that the efficiency for a single spark discharge under static conditions is the same as for a train of sparks with the tunnel in operation at the same static pressure, the efficiency can be taken as 3.8 percent (see table 3) and the power input to the flow will have been approximately 5.3 W. This represents the total power added to the flow, so that the power into the boundary layer is again only a fraction of this value.

REFERENCES

1. Braslow, A. L.; Hicks, R. M.; and Harris, R. V., Jr.: Use of Grit-Type Boundary-Layer-Transition Trips on Wind-Tunnel Models. NASA TN D-3579, 1966.

2. Van Driest, E. R.; and McCauley, W. D.: The Effect of Controlled Three-Dimensional Roughness on Boundary-Layer Transition at Supersonic Speeds. J. Aero/Space Sci., vol. 27, no. 4, April 1960, pp. 261-271.

3. Klein, E. J.: Liquid Crystals in Aerodynamic Testing. Astro. & Aero., vol. 6, no. 7, July 1968, pp. 70-73.

4. Daugherty, J. C.; and Hicks, R. M.: Measurement of Local Skin Friction Downstream of Grit-Type Boundary-Layer-Transition Trips at M = 2.17 and Zero Heat Transfer. AIAA J., vol. 8, no. 5, May 1970, pp. 940-941.

5. Kovasznay, L. S. G.; Komoda, H.; and Vasudeva, B. R.: Detailed Flow Field in Transition. Proc. 1962 Heat Transfer and Fluid Mechanics Inst., Stanford University Press, 1962, pp. 1-26.

6. Hama, F. R.; and Nutant, J.: Detailed Flow-Field Observations in the Transition Process in a Thick Boundary Layer. Proc. 1963 Heat Transfer and Fluid Mechanics Inst., Stanford University Press, 1963, pp. 77-93.

7. Mitchner, M.: Propagation of Turbulence from an Instantaneous Point Disturbance. J. Aero. Sci., vol. 21, no. 5, May 1954, pp. 350-351.

8. Schubauer, G. B.; and Klebanoff, P. S.: Contributions on the Mechanics of Boundary-Layer Transition. NACA Rep. 1289, 1956.

9. Elder, J. W.: An Experimental Investigation of Turbulent Spots and Breakdown to Turbulence. J. Fluid Mech., vol. 9, part 2, Oct. 1960, pp. 235-246.

10. Schubauer, G. B.; and Skramstad, H. K.: Laminar-Boundary-Layer Oscillations and Transition on a Flat Plate. NACA Rep. 909, 1948.

11. Laufer, J.; and Vrebalovich, T.: Stability and Transition of a Supersonic Laminar Boundary Layer on an Insulated Flat Plate. J. Fluid Mech., vol. 9, part 2, Oct. 1960, pp. 257-299.

12. Kendall, J. M., Jr.: Supersonic Boundary Layer Stability Experiments. Proc. Boundary Layer Transition Study Group Meeting, Aug. 1967, Aerospace Corp., San Bernardino, Calif. (Aerospace Rep. TR-0158 (S3816-63)-1, Vol. II, pp. 10-1 – 10-8).

13. James, C. S.: Observations of Turbulent-Burst Geometry and Growth in Supersonic Flow. NACA TN 4235, 1958.

14. Klein, E. J.: A Planview Shadowgraph Technique for Boundary-Layer Visualization. AIAA J., vol. 8, no. 5, May 1970, pp. 963-965.

15. Van Driest, E. R.: Problem of Aerodynamic Heating. Aero. Eng. Rev., vol. 15, no. 10, Oct. 1956, pp. 26-41.

16. Chapman, D. R.; Kuehn, D. M.; and Larson, H. K.: Investigation of Separated Flows in Supersonic and Subsonic Streams with Emphasis on the Effect of Transition. NACA Rep. 1356, 1958.

17. Sedov, L. I.: Point Explosion Taking Counter-Pressure Into Account. Similarity and Dimensional Methods in Mechanics. Fourth ed., Academic Press, New York, 1959, pp. 238-251.

NASA-Langley, 1971 — 1 A-3673

05U 001 26 51 3DS 71147 00903
AIR FORCE WEAPONS LABORATORY /WLOL/
KIRTLAND AFB, NEW MEXICO 87117

ATT E. LOU BOWMAN, CHIEF, TECH. LIBRARY

"The aeronautical and space activities of the United States shall be conducted so as to contribute . . . to the expansion of human knowledge of phenomena in the atmosphere and space. The Administration shall provide for the widest practicable and appropriate dissemination of information concerning its activities and the results thereof."

—NATIONAL AERONAUTICS AND SPACE ACT OF 1958

NASA SCIENTIFIC AND TECHNICAL PUBLICATIONS

TECHNICAL REPORTS: Scientific and technical information considered important, complete, and a lasting contribution to existing knowledge.

TECHNICAL NOTES: Information less broad in scope but nevertheless of importance as a contribution to existing knowledge.

TECHNICAL MEMORANDUMS: Information receiving limited distribution because of preliminary data, security classification, or other reasons.

CONTRACTOR REPORTS: Scientific and technical information generated under a NASA contract or grant and considered an important contribution to existing knowledge.

TECHNICAL TRANSLATIONS: Information published in a foreign language considered to merit NASA distribution in English.

SPECIAL PUBLICATIONS: Information derived from or of value to NASA activities. Publications include conference proceedings, monographs, data compilations, handbooks, sourcebooks, and special bibliographies.

TECHNOLOGY UTILIZATION PUBLICATIONS: Information on technology used by NASA that may be of particular interest in commercial and other non-aerospace applications. Publications include Tech Briefs, Technology Utilization Reports and Technology Surveys.

Details on the availability of these publications may be obtained from:

SCIENTIFIC AND TECHNICAL INFORMATION OFFICE

NATIONAL AERONAUTICS AND SPACE ADMINISTRATION

Washington, D.C. 20546